Hindawi
Wireless Communications and Mobile Computing
Volume 2022, Article ID 3384362, 9 pages
https://doi.org/10.1155/2022/3384362

Research Article

Channel Modelling for V2V Highway Scenario Based on Birth and Death Process

Yi Feng, Ning Ge, Xiaoming Tao, Qiwei Song, and Tao Xiang

Department of Electronic Engineering, Tsinghua University, Beijing 100084, China

Correspondence should be addressed to Yi Feng; fengyi12@chinaunicom.cn

Received 14 December 2021; Accepted 15 February 2022; Published 14 March 2022

Academic Editor: Li Zhu

Vehicle-to-vehicle (V2V) communication has been widely researched recently since the potential abilities of improving traffic efficiency and reducing accident rates. Since the high vehicle mobility, a huge number of accidents happen on highway. So, it is necessary to study the highway channel characteristic to ensure the driving safety. Due to the high speed of vehicles, there exists serious nonstationarity of highway channel, leading to the dissatisfaction of the wide-scene stationary uncorrelated scattering (WSSUS) assumption. Thus, a distant channel model is needed. In this paper, we carried out a measurement campaign of highway channel. Based on the measured data, we conduct a birth and death channel model, which is depicted by Markov chain. We propose the first-order model and the second-order model, respectively. The steady probabilities and transition probabilities are given. To compare the two models, we utilize the multipath living time and Kullback-Leibler (KL) distance. What is more, autocorrelation function (ACF) is used to describe the nonstationarity.

1. Introduction

Vehicles have been an important role in people's life. However, more and more traffic accidents occur with the rapid increase of vehicle ownership. According to the data provided by the World Health Organization (WHO), over 1.25 million people are killed in traffic accidents, and tens of millions are injured or disabled every year. Therefore, how to deal with the problems caused by vehicles is imminent [1]. With the rise of intelligent transportation, information technology and automobile industry are becoming deeply integrated, and vehicle-to-everything (V2X) has been an important part of intelligent transportation system (ITS), which can connect vehicles with surrounding vehicles, people, transportation infrastructures, and cloud. As a structural part of V2X, V2V communication systems have drawn great attention for the potential to reduce accident rates and improve traffic efficiency [2, 3].

Dedicated short-range communication (DSRC) and cellular vehicle-to-everything (C-V2X) are the two main technologies of V2X. DSRC is proposed by the United States based on IEEE 802.11p. The communication based on DSRC can be achieved without the cellular network. It has been in development for a long time and has been promoted in the United States as the main solution of V2X, but its commercial progress is not very well, and the evolution route is not clear for new applications such as autodriving [4]. C-V2X is designed by the third-generation partnership projection (3GPP) based on the fourth-generation (4G) mobile communication technology, which was completed in 2016. C-V2X can utilize the existing cellular network infrastructure to reduce deployment costs and provide low latency, high reliability, high transmission rates, and secure communication in high-speed mobile environments. This contributes to a better application for C-V2X in some countries than DSRC.

As the medium of transmitted information, wireless channel is the basis of wireless communication system design [5]. Knowledge of the propagation channel is vital for V2V communication systems designers since its properties will ultimately dictate system performance. Highways are commonly used for people to travel, and the vehicles are fast-moving. Accordingly, it is very important to accurately describe the channel characteristics of highway to

Figure 1: The photo of measurement scenario.

Table 1: The parameter configuration of measurement system.

Parameter	Value
Carrier frequency	5.9 GHz
Bandwidth	20 MHz
Transmit power	27 dBm
Transmit signal	OFDM
Transmit antenna	Omnidirectional antenna
Receiving antenna	Omnidirectional antenna
The height of antenna	2 m
SIMO	1×2
Antenna spacing	2 wavelengths

ensure people's safety [6]. Measurement and modeling are the most efficient ways to get the accurate channel characteristics for the link-level simulation and system-level design. However, unlike traditional cellular network channel, V2V channel varies over time and does not satisfy the assumption of wide-scene stationary uncorrelated scattering (WSSUS). Thus, distinct channel models are required.

In the existing literatures, several works have studied the influence of the velocity and direction of transmitters, receivers, and scatterers on nonstationarity of V2V channel, but fewer papers deal with the nonstationarity of highway. Sen and Matolak described measurements and results of delay spread, amplitude statistics, and correlations for several V2V scenarios at 5GHz in [7]. In [8], a nonstationary channel model considering mobile scatters for street wideband was proposed. In [9], the influence of velocity variation of both receivers and moving scatters on nonstationary channel was investigated. In [10], the impacts of antenna array rotation were incorporated for a three-dimensional channel model, and the stationarity regions of suburban, urban, and underground parking environments were provided in [11]. Based on multiple-input and multiple-output (MIMO) V2V communication, the research in [12] presented a three-dimensional (3D) wideband geometry-based channel model. From the aspect of correlation, the authors in [13] analyzed the nonstationary V2V channel using the time-variant temporal correlation function (TCF) and derived the closed-form TCF expression for nonline-of-sight (NLoS) scenarios. In [14], the local region of stationarity is adopted to analyze the nonstationarity of V2V radio channels in seven scenarios.

In this paper, the birth and death progress is used to model the highway V2V channel based on Markov chain. Steady-state probability and transition probability of the first-order model and the second-order model are given, which can be used to simulate the nonstationary channel. We also utilize the time autocorrelation function (ACF) to describe the nonstationary features. To demonstrate the performance of the models, we compare the lifetime fitting degree between measured data and simulated data, respectively, and further verify of the first-order model and second-order model by adopting KL distance.

The remainder of this paper is outlined as follows. In the next section, we introduce our measurement campaign and data processing method separately. Then, our channel models are described in Section 3. The validation of the models is in Section 4. Finally, the conclusions are drawn in Section 5.

2. Channel Measurement Campaign

2.1. Scenario and Equipment of Measurement. The research group measured the V2V channel of highway in Shanghai Lingang autonomous and informationalized vehicle integrative testing and demonstration zone, China. The measured highway road was built as the same standard as common highway scenarios, including the guideposts and plants on both sides of the road. The transmitting vehicle and the receiving vehicle moved towards from an initial distance of about 600 meters and then moved away after meeting. The antennas were located on the top of the vehicles. The measurement scenario is shown in Figure 1.

The measurement system concludes vector signal generator, spectrum analyzer, transceiver antenna system, and synchronization unit. Vector signal generator R&S SMW200A and spectrum analyzer R&S FSW 67 are used at Tx and Rx to compose a frequency domain channel sounder. GPS timer rubidium clocks are used to provide 10 MHz reference clock. A single-input multiple-output (SIMO) mode is used in this measurement, with two antennas at Rx. The gain of each antenna is 6 dBi, and each antenna is omnidirectional. The distance between the receiving antennas is about 10 cm, and the top of antenna is 2 m from ground. The total transmitter power of the vector signal generator and the power amplifier is 21 dBm, so the total transmitted power is 27 dBm due to the antenna gain. The signal used for measurement is orthogonal frequency division multiplexing (OFDM) signal containing 2560 subcarriers, each signal has 256 zero-complementing subcarriers, that is, the effective number of subcarriers is 2048. The measured frequency point, bandwidth, transmission power, and other parameters are configured based on 3GPP TR 36.885, which are according to V2X testing standard. The detail of parameter configuration is shown in Table 1.

2.2. Extraction of the Channel Parameters. After data containing channel information is obtained from measurement campaign, the channel parameters need to be extracted.

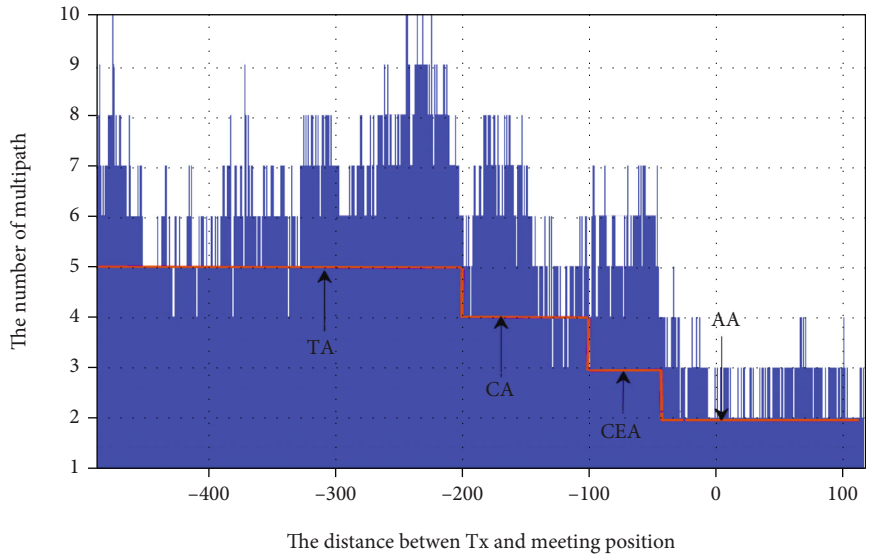

Figure 2: The variation of multipath distribution with the distance.

Table 2: Division of different areas.

Area	Distance	Average multipath number
TA	[-500 m, -200 m]	5
CA	[-200 m, -100 m]	4
CEA	[-100 m, -40 m]	3
AA	[-40 m,0 m]	2

The first and the most important step is to get channel impulse response (CIR), which contains large-scale fading information and small-scale fading information, as shown in

$$h(t,\tau) = \sum_{l=0}^{L} a_l(t) e^{-j2\pi f_D(t)t} \delta(\tau - \tau_l(t)), \quad (1)$$

where τ is time delay and L is the number of resolvable multipaths. $a_l(t)$, $f_D(t)$, and $\tau_l(t)$ represent amplitude, doppler shift, and time delay of the lth resolvable multipath at instant time t, respectively. $\delta(\tau)$ denotes the Dirac delta function. It can be seen from Equation (1) that CIR contains a variety of important channel parameters, such as path loss, delay spread, and Doppler spread. Thus, the correct extraction of CIR will affect the accuracy of subsequent channel analysis. The following steps are the methods to extract CIR:

(1) Convert the collected intermediate frequency (IF) signal into baseband signal by downconversion and low-pass filtering

(2) Get the original CIR by sliding correlation between the resulting baseband signal and the transmitted OFDM signal

(3) Use precise synchronization, coarse synchronization, and the addition of window function to combat the energy leakage of CIR

(4) Get final CIR in the time domain by inverse Fourier transferring

After CIR is obtained, effective multipath recognition is required to extract multipath components. Denoising and multipath searching are the two steps to identity effective multipaths:

(1) Denoising: there are both valid multipath components and invalid noise components in the measured CIR, which are distinguished by setting noise threshold. In order to avoid the influence of the fixed value noise threshold in the decision when the signal-to-noise ratio (SNR) is low or the noise fluctuate greatly, we adopt a dynamic noise threshold that retains the taps whose multipath power is higher than the noise threshold and forces the taps below the noise threshold to zero

(2) Multipath searching: the local maximum method is used to search multipath. This step is to remove the noise "burr" which is higher than the noise decision threshold and further improve the accuracy of multipath extraction. Firstly, the maximum power difference is defined as ΔP, which represents the acceptable minimum power difference between the peak and the neighbour valley. Then, search for the power and location of the peak above the noise threshold, and whether the peak is a noise "burr" is determined by comparing each peak power with ΔP

Based on the extracted multipath, the variation of multipath distribution with the distance is shown in Figure 2.

In Figure 2, the x-axis is the distance between the transmitting vehicle and the meeting point; the y-axis is the number of distinguishable multipaths at each point. We divide the whole measurement region into 4 parts according to the dynamic change of effective multipath [15]: toward area (TA), Similar to the first-order model (AA), as shown in Table 2.

Table 3: Comparison table of states of second-order Markov chain.

State	The relationship with "0," "1"	Physical meaning
1	$\begin{cases} z_l(t\text{-}1) = 0 \\ z_l(t) = 0 \end{cases}$	Both of the adjacent time do not exist multipath.
2	$\begin{cases} z_l(t\text{-}1) = 0 \\ z_l(t) = 1 \end{cases}$	There exist multipath at the current time but no multipath at the previous time.
3	$\begin{cases} z_l(t\text{-}1) = 1 \\ z_l(t) = 0 \end{cases}$	There exist multipath at the previous time but no multipath at the current time.
4	$\begin{cases} z_l(t\text{-}1) = 1 \\ z_l(t) = 1 \end{cases}$	Both of the adjacent exist multipath.

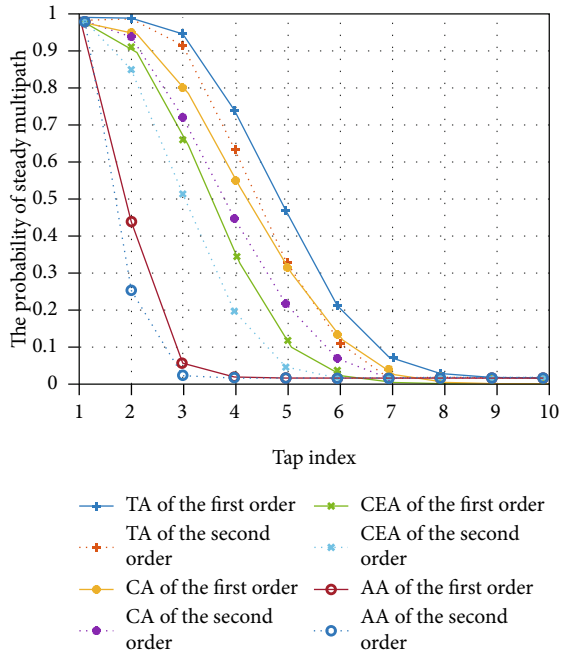

Figure 3: The comparison of the probability of "on" state in each region.

3. Channel Modelling

3.1. Birth and Death Progress for Nonstationary Channel. In general, the tap delay line (TDL) model based on Equation (1) can be used to describe the multipath variation characteristics of wireless propagation environment, provided that the scenario satisfies WSSUS assumption [16]. But in V2V, the fast-moving vehicles and low transmitting and receiving antenna heights will cause the channel characteristics change frequently and rapidly, so that the channel no longer meets the WSSUS assumption, leading to a seriously nonstationary. As a result, the number and intensity of multipath components often change. In this scenario, the traditional TDL model cannot describe the multipath variation accurately; however, an improved TDL model based on birth and death progress can be used to describe the nonstationary channel, as shown in Equation (2) [17]:

$$h(t,\tau) = \sum_{l=0}^{L} z_l(t) a_l(t) e^{-j2\pi f_D(t)t} \delta(\tau - \tau_l(t)). z_l(t) \in \{0,1\}. \tag{2}$$

The difference between Equation (1) and Equation (2) is $z_l(t)$, which controls the "ON" or "OFF" of the lth path, representing the persistence of multipath in random progress. For example, for a sequence that $z_l(t) = 111001$, it means that the multipath can be detected in the first three intervals, then disappears at the following two intervals, and at the end of time, it can be detected again.

For the tap persistence process, we use Markov chain to model the birth and death progress, which is frequently used in continuous process modelling. We developed first-order two-state Markov chains and second-order four-state Markov chains, respectively. For the first-order Markov chain, the steady-state probability matrix and transition probability matrix are used to characterize it, as shown in Equations (3) and (4), respectively [18]:

$$SS_1 = \begin{bmatrix} S_{1,0} \\ S_{1,1} \end{bmatrix}, \tag{3}$$

$$TS_1 = \begin{bmatrix} P_{1,00} & P_{1,01} \\ P_{1,10} & P_{1,11} \end{bmatrix}, \tag{4}$$

where $S_{1,i}$ represents the steady probability of state i, $P_{1,ij}$ represents the probability of transition from state i to state j. There are two states "0" and "1" in the first-order Markov chain, which denote "OFF" and "ON" of multipath, respectively. Note that because SS_1 and TS_1 are probability matrix, we have the Equation of $\begin{cases} S_{1,0} + S_{1,1} = 1 \\ P_{1,i0} + P_{1,i1} = 1 \end{cases}$.

Due to the rapid change of measured channel, the channel state is less correlated. Considering higher-order model can simultaneously observe channel states in longer time to track the channel variations deeper in the past, we employ the second-order Markov chain to model the V2V channel, but the modelling complexity will also increase. There are four states for the second order Markov chain, which are

Table 4: Channel model for the first-order Markov chain.

	Taps	Delay (μs)	$S_{1,0}$	$S_{1,1}$	$P_{1,00}$	$P_{1,11}$
TA	1	0	0	1	0	1
	2	0.43	0.0023	0.9977	0.1017	0.9979
	3	0.76	0.0461	0.9539	0.3102	0.9666
	4	0.92	0.2570	0.7430	0.5860	0.8568
	5	0.79	0.5353	0.4647	0.7393	0.6996
CA	1	0	0	1	0	1
	2	0.49	0.0309	0.9691	0.2392	0.9757
	3	0.98	0.1956	0.8044	0.5839	0.8988
	4	0.90	0.4550	0.5450	0.7742	0.8115
CEA	1	0	0	1	0	1
	2	0.39	0.0819	0.9181	0.2293	0.9312
	3	0.61	0.3396	0.6604	0.5578	0.7727
AA	1	0	0	1	0	1
	2	0.15	0.5664	0.4336	0.6640	0.5611

shown in Table 3. Similar to the first-order model, SS_2 and TS_2 are the steady state probability matrix and transition probability matrix, as shown in

$$SS_2 = \begin{bmatrix} S_{2,1} & S_{2,2} \\ S_{2,3} & S_{2,4} \end{bmatrix}, \tag{5}$$

$$TS_2 = \begin{bmatrix} P_{2,11} & P_{2,12} & 0 & 0 \\ 0 & 0 & P_{2,23} & P_{2,24} \\ P_{2,31} & P_{2,32} & 0 & 0 \\ 0 & 0 & P_{2,43} & P_{2,44} \end{bmatrix}, \tag{6}$$

and we have

$$\begin{cases} S_{2,1} + S_{2,2} + S_{2,3} + S_{2,4} = 1, \\ P_{2,i1} + P_{2,i2} = 1 \ (i \in \{1, 3\}), \\ P_{2,j3} + P_{2,j4} = 1 \ (j \in \{2, 4\}). \end{cases} \tag{7}$$

3.2. Channel Model Based on Markov Chain. In this section, we utilize the first-order Markov chain and the second-order Markov chain to model the V2V highway scenario channel in the area of TA, CA, CEA, and AA, respectively.

The comparison of the multipath steady probabilities in various regions is shown in Figure 3. In Figure 3, the results of the two models are shown, and the probabilities are $S_{1,1}$ and $S_{2,4}$ actually. Since we always select the first arrival diameter as tap 1, the probabilities of tap 1 for each subregion are fixed to 1. Figure 3 indicates that $S_{1,1}$ and $S_{2,4}$ of each zone decrease with the increase of multipath delay, which means the long-delay paths have a higher probability of "OFF" state. This is because of the long multipath transmission time and the large number of reflections, resulting a low energy when echo reaches the receiving end and be flooded by noise, showing that the tap does not exist multipath. By observing the curves of each area, it can be found that the curve at tap 2 is denser than others, which means that each area has a higher multipath survival probability at the second tap. It may because the multipaths of the second tap are generated by fixed scatterers around the test scenario, such as trees, fences, and signs on both sides of the road. What is more, through the probabilities of different regions at the same tap, we can know that TA has the highest probability, followed by CA, CEA, and AA. This result indicates that the farther multipaths are more likely to survive, while those near the meeting position have a weaker life. This is because the highway environment is more spacious, and the channel nonstationarity is not particularly obvious when the vehicles are far away. When the vehicles are close to each other, the nonstationarity is exacerbated due to the relative motion between the vehicles, resulting in lower survival probability. We can also find that the second-order model generally has a lower probability of survival than the first-order model; the reason is the first-order model only considers the current state, while the higher-order model tracks several moments, which makes the prediction more accurate. Table 4 and Table 5 provide the parameters of the two models, respectively. The values not to be listed can be calculated by $P_{1,i0} + P_{1,i1} = 1$, $P_{2,i1} + P_{2,i2} = 1 (i \in \{1, 3\})$, and $P_{2,j3} + P_{2,j4} = 1 (j \in \{2, 4\})$.

From Figure 3, it can be observed that the probability distributions of TA and CA regions are approximately subordinated to the trigonometric function, while those of CEA and AA regions are subordinated to the exponential distribution due to the serious nonstationarity. Thus, we fit $S_{1,1}$ and $S_{2,4}$ of TA and CA regions as Fourier function, and exponential fitting of CEA and AA regions are carried out, as shown in

$$P(l) = a_0 + a_1 \cos(lw) + b_1 \sin(lw), \tag{8}$$

$$P(l) = m \exp(nl), \tag{9}$$

where a_0, a_1, b_1, w, m, and n are fitting parameters and l is the tap index. The value of fitting parameters is shown in Table 6.

3.3. The Correlation Characteristic. Under the assumption of WSSUS, the channel correlation is only related to time interval rather than the time instant. But in actual V2V scenario, the movement of scatters and vehicles will cause the channel to change with time, which is leading to time-variable correlation. To characterize the nonstationarity from the point of view of correlation, the autocorrelation function (ACF) is used to depict it, as shown in

$$ACF(\tau) = E\{h^*(t)h(t+\tau)\}, \tag{10}$$

where τ is the time interval and $h^*(t)$ is complex conjugate of $h(t)$. According to Equation (10), we can see that ACF indicates the similarity between the CIR at time instant t and time delay τ. That is to say, a higher ACF means a stronger dependence of $h(t+\tau)$ on $h(t)$.

Table 5: Channel model for the second-order Markov chain.

	Taps	Delay (μs)	$S_{2,1}$	$S_{2,2}$	$S_{2,3}$	$S_{2,4}$	$P_{2,11}$	$P_{2,23}$	$P_{2,31}$	$P_{2,44}$
TA	1	0	0	0	0	1	0	0	0	1
	2	0.43	0.0002	0.0021	0.0021	0.9956	0	0.0755	0.1132	0.9981
	3	0.76	0.0143	0.0318	0.0318	0.9221	0.4360	0.1581	0.2537	0.9709
	4	0.92	0.1506	0.1064	0.1064	0.6366	0.6697	0.3401	0.4676	0.8897
	5	0.79	0.3957	0.1396	0.1396	0.3251	0.8020	0.4320	0.5612	0.7561
CA	1	0	0	0	0	1	0	0	0	1
	2	0.49	0.0074	0.0235	0.0235	0.9456	0.3091	0.1200	0.2172	0.9781
	3	0.98	0.1142	0.0814	0.0814	0.7230	0.6671	0.2971	0.4671	0.9210
	4	0.90	0.3523	0.1026	0.1028	0.4423	0.8395	0.4294	0.5504	0.8674
CEA	1	0	0	0	0	1	0	0	0	1
	2	0.39	0.0188	0.0631	0.0631	0.8549	0.3133	0.1936	0.2043	0.9404
	3	0.61	0.1894	0.1500	0.1503	0.5103	0.6238	0.3621	0.4745	0.8122
AA	1	0	0	0	0	1	0	0	0	1
	2	0.15	0.3761	0.1903	0.1904	0.2433	0.6918	0.4940	0.6091	0.6039

Table 6: The value of fitting parameters.

Region	The first-order model	The second-order model
	$[a_0, a_1, b_1, w]$	
TA	[0.485, 0.430, 0.327, 0.442]	[0.480, 0.509, 0.227, 0.430]
CA	[0.509, 0.562, 0.015, 0.378]	[0.579, 0.586, -0.258, 0.334]
	$[m, n]$	
CEA	[1.71, -0.412]	[1.804, -0.492]
AA	[2.890, -1.047]	[4.505, -1.503]

Figure 4 illustrates the time varying ACF. We compare ACF of the four subregions at TAP 2. The comparison of TAP 2 and TAP 3 is also given under AA area. There can be found that the correlations are greater than 0.8 in the first 0.5 ms and then dropped to 0.6 at about 0.72 ms, which indicates the nonstationary channel of highway scenario only has strong correlation in a short time. In addition, we can see with the increase of time, the ACF curves decrease rapidly at the first and then change slowly. The is because the multipath component is stronger in the initial period of time, leading to the sharply decline of ACF. When ACF decreases to a certain value, the multipath intensity is negligible compared with direct path, leading to a relatively stable curve. Besides, it is obvious that the strength of direct path is the highest in TA. Through the comparison of TAP 2 and TAP 3, a conclusion can be drawn that the nonstationarity will be aggravated as the increase of multipath delay.

4. Application of Model

Multipath lifetime can be used to describe the possible duration of each potential path, which is of great significance for the studying nonstationary channels. We use T_S as the unit persistent period; the steady-state probabilities and transition probabilities obtained in Section 2 are used to derive the multipath survival time. When the first-order model is adopted, the indicator is mathematically shown in

$$LT_1(n) = S_{1,1} * (P_{1,11})^{n-1} n = 1, 2, 3, \cdots, \quad (11)$$

where n denotes the number of T_S in lifetime. When the second-order model is adopted, the indicator is shown in

$$LT_2(n) = S_{2,4} * (P_{2,44})^{n-2} n = 1, 2, 3, 4, \cdots. \quad (12)$$

According to AA has the most severe nonstationarity in the subregions, we take this area to demonstrate the effectiveness of our models. The real survival time is calculated from the measured data; $LT_1(n)$ and $LT_2(n)$ are calculated according to Equation (11) and Equation (12), respectively. We plot the comparison of the three results in Figure 5.

As shown in the figure, the survival probabilities decrease exponentially with time, which is familiar with the tendency of steady probability. Notice that when n equals to 1 and 2, $LT_1(n)$ equals to $S_{1,1}$ and $S_{2,4}$, respectively. Hence, the value of measured data and the first-order model at the first and second T_S are the same in Figure 5. In addition, most survival paths are concentrated in the first three T_S. Through the comparison between the measured data and the two models, it can be observed that there is little difference between the simulated data and the measured data in the first three T_S. But with the increase of T_S, the second-order model shows a better performance.

In order to further judge the property of the two models, we adopt Kullback-Leibler distance, i.e., KL distance, which can be used to measure the difference between two groups of discrete probability distributions, as shown in Equation (13) [4]:

$$KL = \sum_{i=1}^{M} D(i) \log_2 \left(\frac{D(i)}{S(i)} \right), \quad (13)$$

where $D(i)$ and $S(i)$ are the measured data and model data, respectively, and M is the number of points of calculated data. Note that the smaller of the KL is, the better of the

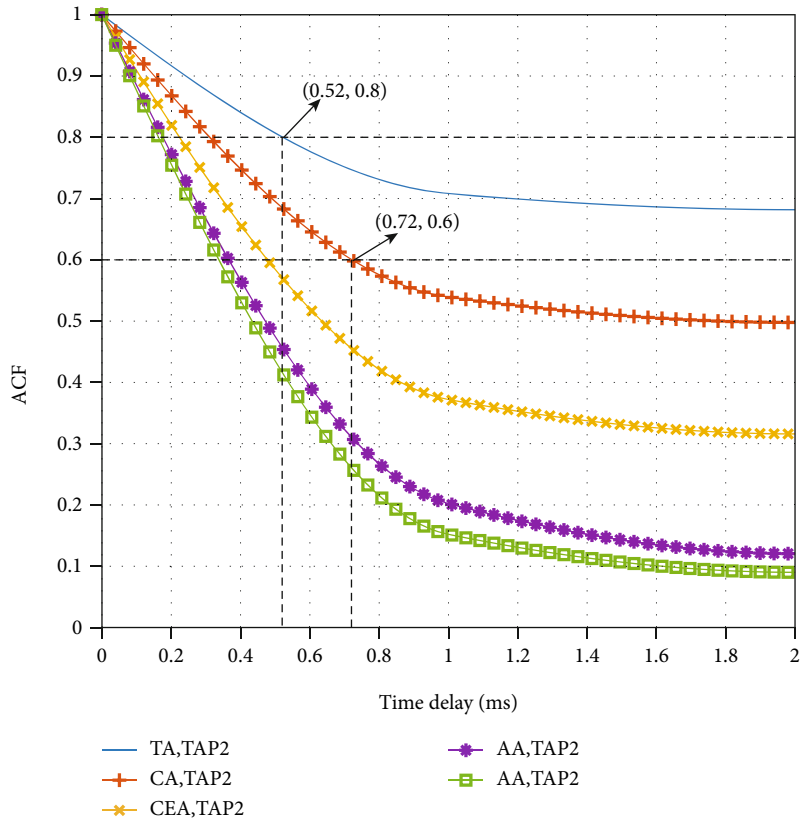

Figure 4: The time varying ACF.

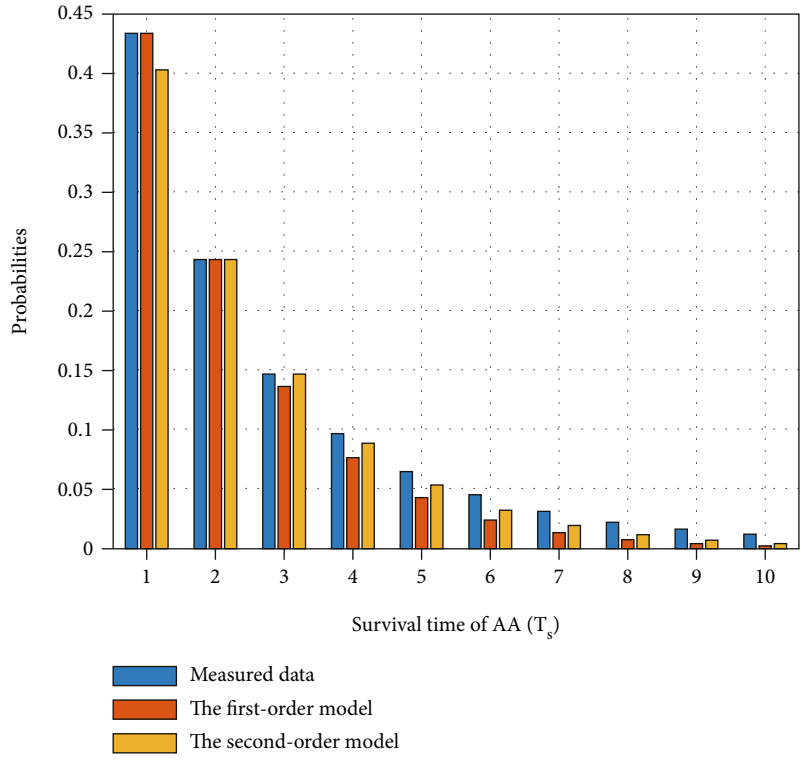

Figure 5: Survival time of AA.

Table 7: KL distance of each area and tap.

Region	The first-order model	The second-order model
TA2	0.0107	0.0029
TA3	0.4616	0.2741
TA4	1.5679	0.7620
TA5	0.8691	0.4237
CA2	0.2760	0.1681
CA3	1.3890	0.7126
CA4	1.4980	0.5966
CEA2	0.5950	0.2699
CEA3	1.0655	0.5071
AA2	0.1498	0.0500

consistency between $D(i)$ and $S(i)$ is. For our model, we take the measured multipath survival time as $D(i)$ and the survival time calculated by the two models as $S(i)$. The KL distances of subregions are shown in Table 7.

It can be seen that both the first-order model and the second-order model have a satisfactory description effect on nonstationary channel. But the performance on the propagation path with longer delay is not as well as those with shorter delay. The reason is the longer delayed multipath components occur more reflexes, which will be affected by the surrounding environment seriously. That is to say, there happens greater uncertainty in propagation process; thus, the model accuracy is reduced. Comparing the lower-order model with the higher-order model, it can be found that each KL distance of the second-order model is smaller than that of the first-order model, which proves the second-order model has better performance. To sum up, to consider the modelling complexity and accuracy at the same time, the first-order model can be adopted for the smaller delay taps, and the second-order model can be adopted for the larger delay taps. It is a way of improving little modelling complexity in exchange for higher modelling accuracy.

5. Conclusions

This paper presents a study on nonstationary characteristic of V2V channel for highway scenario. We conducted a channel measurement campaign of V2V in Shanghai, China; the measurement scheme and data processing method are introduced. To characterize the nonstationary properties, we utilize the birth and death progress based on the first-order and second-order Markov chain. Steady-state probability and transition probability of the two models are provided in this paper, which can be used to simulate the channel. We also give the fitting parameters of the probability of "ON" state in each subregion. Moreover, the autocorrelation function of the channel is provided to indicate the correlation characteristic of time-varying channel. Finally, we use the multipath survival time and KL distance to validate the accuracy of the two models, and compare the performance of the models. The result is both of the two models have good description effect on nonstationary channel, but the second-order model is better for large delay taps. Therefore, we can utilize the first-order model for the small delay taps and the second-order model for the large delay taps to guarantee the accuracy and complexity of channel model at the same time.

Data Availability

The data used to support the findings of this study are currently under embargo, so cannot be made freely available.

Conflicts of Interest

The authors declare that there are no conflicts of interest regarding the publication of this paper.

Acknowledgments

This research was supported by the National Key R&D Program of China under grant 2018YFA0701601.

References

[1] C.-x. Wang, X. Cheng, and D. Laurenson, "Vehicle-to-vehicle channel modeling and measurements: recent advances and future challenges," *IEEE Communications Magazine*, vol. 47, no. 11, pp. 96–103, 2009.

[2] A. Molisch, F. Tufvesson, J. Karedal, and C. Mecklenbrauker, "A survey on vehicle-to-vehicle propagation channels," *IEEE Wireless Communications*, vol. 16, no. 6, pp. 12–22, 2009.

[3] L. Zhu, H. Liang, H. Wang, B. Ning, and T. Tang, "Joint security and train control design in blockchain empowered CBTC system," *IEEE Internet of Things Journal*, vol. SCI, 2021.

[4] C. H. E. N. Shanzhi, H. U. Jinling, S. H. I. Yan, and Z. H. A. O. Li, "Technologies, standards and applications of LTE-V2X for vehicular networks," *Telecommunications Science*, vol. 34, no. 4, pp. 1–11, 2018.

[5] L. Zhu, Y. Li, F. R. Yu, B. Ning, T. Tang, and X. Wang, "Cross-layer defense methods for jamming-resistant CBTC systems," *IEEE Transactions on Intelligent Transportation Systems*, vol. 22, no. 11, pp. 7266–7278, 2020.

[6] Y. Li, L. Zhu, H. Wang, F. R. Yu, and S. Liu, "A cross-layer defense scheme for edge intelligence-enabled CBTC systems against Mit M attacks," *IEEE Transactions on Intelligent Transportation Systems*, vol. 22, no. 4, pp. 2268–2298, 2020.

[7] I. Sen and D. W. Matolak, "Vehicle–vehicle channel models for the 5-GHz band," *IEEE Transactions on Intelligent Transportation Systems*, vol. 9, no. 2, pp. 235–245, 2008.

[8] X. Liang, X. Zhao, S. Li, Q. Wang, and J. Li, "A non-stationary geometry-based scattering model for street vehicle-to-vehicle wideband MIMO channels," in *In 2015 IEEE 26th Annual International Symposium on Personal, Indoor, and Mobile Radio Communications (PIMRC)*, pp. 2239–2243, Hong Kong, China, Sept 2015.

[9] W. Li, X. Chen, Q. Zhu, W. Zhong, D. Xu, and F. Bai, "A novel segment-based model for non-stationary vehicle-to-vehicle channels with velocity variations," *IEEE Access*, vol. 7, pp. 133442–133451, 2019.

[10] J. Bian, C.-X. Wang, J. Huang et al., "A 3D wideband non-stationary multi-mobility model for vehicle-to-vehicle MIMO channels," *IEEE Access*, vol. 7, pp. 32562–32577, 2019.

[11] R. He, O. Renaudin, V.-M. Kolmonen et al., "A dynamic wideband directional channel model for vehicle-to-vehicle communications," *IEEE Transactions on Industrial Electronics*, vol. 62, no. 12, pp. 7870–7882, 2015.

[12] H. Jiang, Z. Zhang, L. Wu, J. Dang, and G. Gui, "A 3-D non-stationary wideband geometry-based channel model for MIMO vehicle-to-vehicle communications in tunnel environments," *IEEE Transactions on Vehicular Technology*, vol. 68, no. 7, pp. 6257–6271, 2019.

[13] Q. Zhu, W. Li, C.-X. Wang et al., "Temporal correlations for a non-stationary vehicle-to-vehicle channel model allowing velocity variations," *IEEE Communications Letters*, vol. 23, no. 7, pp. 1280–1284, 2019.

[14] F. Li, W. Chen, and Y. Shui, "Analysis of non-stationarity for 5.9 GHz channel in multiple vehicle-to-vehicle scenarios," *Sensors.*, vol. 21, no. 11, p. 3626, 2021.

[15] L. Liu, C. Tao, R. Sun, H. Chen, and Z. Lin, "Non-stationary channel characterization for high-speed railway under viaduct scenarios," *Chinese Science Bulletin*, vol. 59, no. 35, pp. 4988–4998, 2014.

[16] N. Hassan, M. Käske, C. Schneider, G. Sommerkorn, R. Thomä, and D. Matolak, "Measurement-based determination of parameters for non-stationary TDL models with reduced number of taps," *IET Microwaves, Antennas & Propagation*, vol. 14, no. 14, pp. 1719–1732, 2020.

[17] D. W. Matolak, "Modeling the vehicle-to-vehicle propagation channel: a review," *Radio Science*, vol. 49, no. 9, pp. 721–736, 2014.

[18] D. W. Matolak, "Channel modeling for vehicle-to-vehicle communications," *IEEE Communications Magazine*, vol. 46, no. 5, pp. 76–83, 2008.